The Singularity Structure of πN Scattering Amplitudes

郑汉青

四川大学

2022 年 9 月 29 日

Talk given at Beijing Institute of High Energy Physics

Contents

Data from partial wave analysis

- The πN scattering $\rightarrow$ one of the most fundamental and important processes in nuclear and hadron physics
- Decades of researches
- Various experiments and phenomena
  ($L_{2I\ 2J}$ convention, $W = \sqrt{s}$, $S_r = 1 - \eta^2$)[SAID: WI 08]

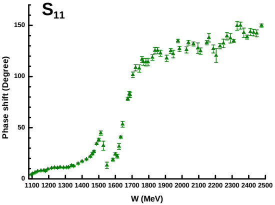

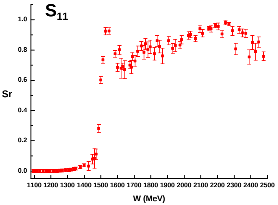

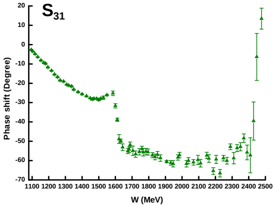
S_{31}
Phase shift (Degree)
W (MeV)
20
10
0
-10
-20
-30
-40
-50
-60
-70
1100 1200 1300 1400 1500 1600 1700 1800 1900 2000 2100 2200 2300 2400 2500

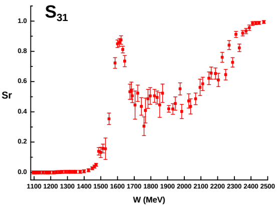
S_{31}
Sr
W (MeV)
1.0
0.8
0.6
0.4
0.2
0.0
1100 1200 1300 1400 1500 1600 1700 1800 1900 2000 2100 2200 2300 2400 2500

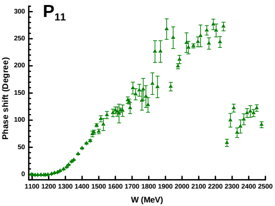
P_{11}
Phase shift (Degree)
W (MeV)
300
250
200
150
100
50
0
1100 1200 1300 1400 1500 1600 1700 1800 1900 2000 2100 2200 2300 2400 2500

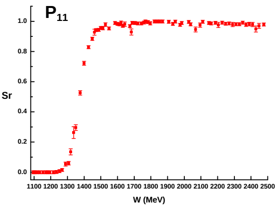
P_{11}
Sr
W (MeV)
1.0
0.8
0.6
0.4
0.2
0.0
1100 1200 1300 1400 1500 1600 1700 1800 1900 2000 2100 2200 2300 2400 2500

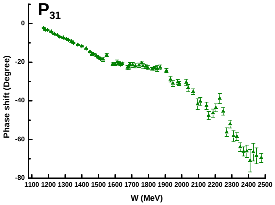
P31
Phase shift (Degree)
W (MeV)

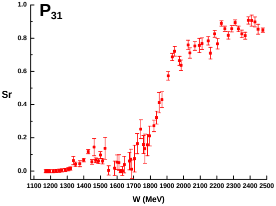
P31
Sr
W (MeV)

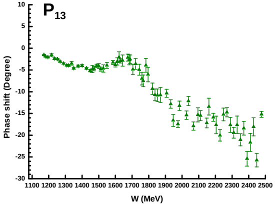
P13
Phase shift (Degree)
W (MeV)

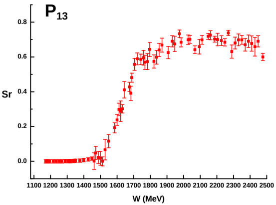
P13
Sr
W (MeV)

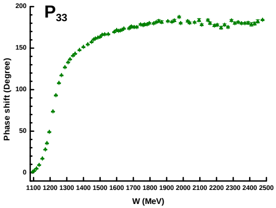
P33
Phase shift (Degree)
200
150
100
50
0
1100 1200 1300 1400 1500 1600 1700 1800 1900 2000 2100 2200 2300 2400 2500
W (MeV)

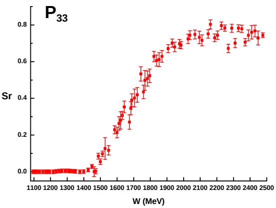
P33
Sr
0.8
0.6
0.4
0.2
0.0
1100 1200 1300 1400 1500 1600 1700 1800 1900 2000 2100 2200 2300 2400 2500
W (MeV)

Theoretical discussions

- Problems to study
  - Low energy properties:
    $\pi N\, \sigma$-term, subthreshold expansions
    [C. Ditsche et. al. 2012 JHEP][Y. H. Chen et. al. 2013 PRD][Hoferichter et. al. 2016 Phys.Rept.]
  - Intermediate resonances: $\Delta(1232)$, $N^*(1440)$, $N^*(1535)\cdots$
- Methods
  - Perturbative calculation
    $O(p^3)$ [J.M. Alarcón et. al. 2012 RPD]; $O(p^4)$ [Y. H. Chen et. al. 2013 PRD]
  - Couple channel Lippmann-Schwinger Equation
    [O. Krehl et. al. 2000 PRC]
  - Dispersion technique
    [A. Gasparyan and M.F.M. Lutz 2010 NPA]
  - Roy-Steiner equation
    [C. Ditsche et. al. 2012 JHEP][Hoferichter et. al. 2016 Phys.Rept.]

S_{11} AND P_{11} CHANNELS

- S_{11} channel ($L_{2I\ 2J}$ convention): $N^*(1535)$
  [N. Kaiser et. al. 1995 PLB][J. Nieves et. al. 2000 PRD]
  - lies above the P- wave first resonance $N^*(1440)$
  - large couple channel effects with πN and ηN
- P_{11} channel: $N^*(1440)$ (Ropper resonance), various puzzles
  - low mass, large decay width, coupling to σN channel... [O. Krehl et. al. 2000 PRC]
  - two-pole structure? [R. A. Arndt et. al. 1985 PRD]
  - second sheet complex branch cut in P_{11} channel?
    [S. Ceci et. al. 2011 PRC]
- A method is needed to examine the relevant channels carefully and to exhume more physics behind
  - low energy
  - model independent

PKU representation

- Production representation, or PKU representation: elastic two-body scattering amplitude

$$S = \prod_i S_i \times S_{cut}$$

- S_i: pole terms, $S_{cut} = e^{2i\rho(s)f(s)}$: left-hand cuts and right hand inelastic cut – background.

$$f(s) = \frac{s}{2\pi \mathrm{i}} \int_{\mathrm{L}} ds' \frac{\mathrm{disc}f(s')}{(s'-s)s'} + \frac{s}{2\pi \mathrm{i}} \int_{\mathrm{R}'} ds' \frac{\mathrm{disc}f(s')}{(s'-s)s'}$$

- $f(0) \equiv 0$ [Z. Y. Zhou and H. Q. Zheng 2006 NPA]

PKU representation

- $f(s)$ perturbatively calculated, poles as parameters (input or fit)
- Corresponding to the Ning Hu representation in QM
  [N. Hu 1948 PR] [T. Regge 1958 Nuovo Cimento]
- Advantages
  - rigorous and universal
  - separated $S \to$ additive phase shift
  - sensitive to (not too) distant poles
  - <u>definite sign of the phase shifts</u> $\to$ figuring out hidden contributions
- Applications
  - the $\pi\pi$ elastic scattering $\to$ existence of the σ particle $(f_0(500))$
    [Z. G. Xiao and H. Q. Zheng 2001 NPA]
  - the πK elastic scattering $\to$ κ resonance $(K^*(800))$
    [H. Q. Zheng et. al. 2004 NPA]
  - resonance sum rules (narrow width approximation)
    [Guo Z.H. et al., JHEP 2007 NPA]

Branch cut structure of partial wave πN elastic scattering amplitude

[S. W. MacDowell 1959 PR][J. Kennedy and T. D. Spearman 1961 PR]

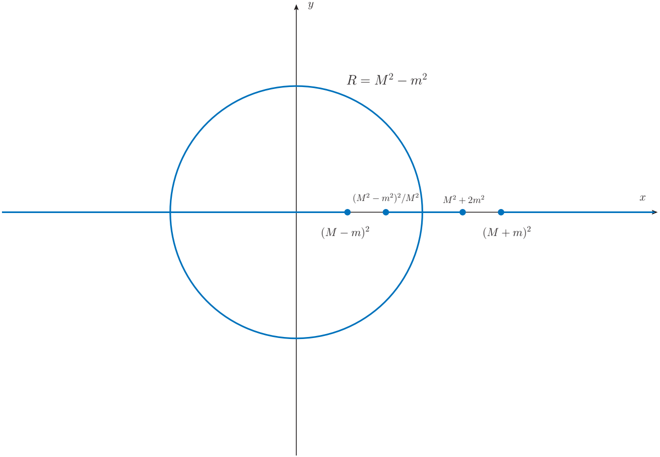

Phase shift components

- PKU representation → conventionally additive phase shift
- Phase shift contributions
  - bound states → negative phase shift
  - virtual states (usually hidden !) → positive phase shift
  - resonances → positive phase shift
  - left hand cut → (empirically) negative phase shift (proved in quantum mechanical potential scatterings)

    [T. Regge 1958 Nuovo Cimento]

Background phase shifts

Estimated both at $O(p^2)$ and $O(p^3)$ level. (Tree level plotted). $L_{2I\ 2J}$ convention, $W = \sqrt{s}$, data: green triangles [SAID: WI 08]

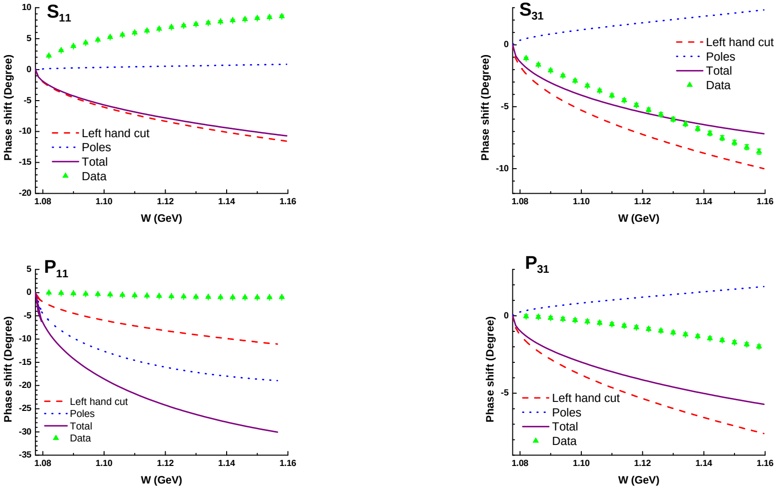

Background phase shifts

$L_{2I\ 2J}$ convention, $W = \sqrt{s}$, data: green triangles [SAID: WI 08]

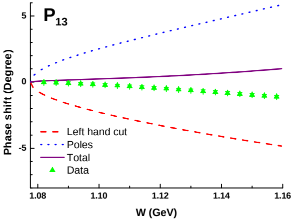

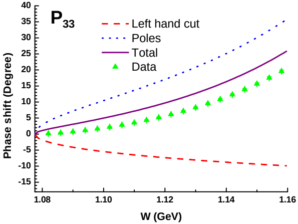

Discrepancies in S_{11} and P_{11} channels

Large missing positive contributions

P_{11}:

- Analytical continuation: $S^{\mathrm{II}} = 1/S^{\mathrm{I}}$.
  Second sheet poles $\rightarrow$ first sheet zeros.
- Expansion: $S^{\mathrm{I}} \sim a/(s - M_N^2) + b + \cdots$
- Arbitrary non-zero $b \rightarrow$ the virtual state
- Perturbation calculation $\rightarrow$ virtual state at 976 MeV; fit $\rightarrow$ 980 MeV

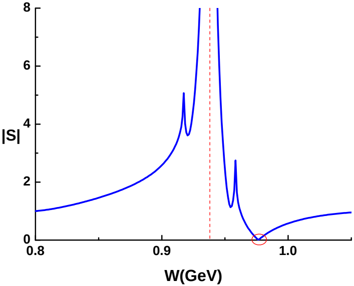

Finding S_{11} hidden pole

$O(p^2)$[YF Wang et al., 2018 EPJC];
$O(p^3)$[YF Wang et al., 2019 CPC]

- Hidden pole $\to$ a "crazy resonance" below threshold $0.895(81)(2) - 0.164(23)(4)i$ GeV.

s_c (GeV^2)	Pole position (MeV)	χ^2/d.o.f
-0.08	$814(3) - i\,141(8)$	1.46
-1.00	$882(2) - i\,190(4)$	1.31
-9.00	$960(2) - i\,192(2)$	1.14
-25.0	$976(2) - i\,187(1)$	1.14

Table 2: The S_{11} hidden pole fit with different choices of s_c.

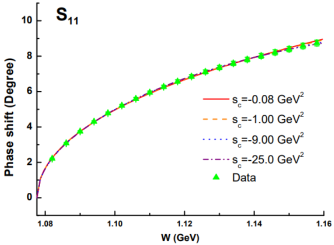

$N^*(890)$ pole in N/D method

Li QZ et al., 2022, Chin. Phys. C

$$T(s) = N(s)/D(s)\ . \tag{1}$$

where :

- D(s) only contains right hand cut,leading: $\mathrm{Im}_R[D(s)] = -\rho(s)N(s)$;
- N(s) contains left cuts and pole,and: $\mathrm{Im}_L[N(s)] = \mathrm{Im}_L[T(s)]D(s)$.

According to dispersion relation:

$$\begin{aligned} D(s) &= 1 - \frac{s-s_0}{\pi}\int_R \frac{\rho(s')N(s')}{(s'-s)(s'-s_0)}ds'\ , \\ N(s) &= N(s_0) + \frac{s-s_0}{\pi}\int_L \frac{D(s')\mathrm{Im}_L[T(s')]}{(s'-s)(s'-s_0)}ds'\ . \end{aligned} \tag{2}$$

$\mathrm{Im}_L T$ as an input.

$$N(s) = N(s_0) + \tilde{B}(s,s_0) + \frac{s-s_0}{\pi}\int_R \frac{\tilde{B}(s,s')\rho(s')N(s')}{(s'-s_0)(s-s')}ds' \tag{3}$$

$$\tilde{B}(s,s') = \frac{s-s'}{\pi}\int_L \frac{\mathrm{Im}_L T(\tilde{s})}{(\tilde{s}-s)(\tilde{s}-s')}d\tilde{s}$$

Analytic continuation:

$$D^{\mathrm{II}}(s) = D(s) + 2i\rho N(s)\ ,\quad N^{\mathrm{II}}(s) = N(s)\ , \tag{4}$$

A toy model calculation

$$N(s) = \sum_i \frac{\gamma_i}{s - s_i} \ , \tag{5}$$

$$D(s) = 1 - \frac{s - s_0}{\pi} \int_R \frac{\rho(s')N(s')}{(s' - s)(s' - s_0)} ds' \ . \tag{6}$$

	Case I	*Case* II
s_1	0	$-m_N^2$
γ_1 (GeV^2)	0.79	1.34
$\sqrt{s_{pole}}$(GeV)	0.810 - 0.125i	0.788 - 0.185i

表: Subthreshold pole locations using input Eq. (5).

.

$\mathcal{O}(p^2)$ calculation

The cuts structure of πN partial wave amplitudes:

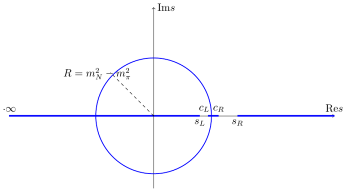

Partial wave projection of χPT amplitudes encounter a severe problem at $s = 0$,

$$\mathcal{T}\big[\mathcal{O}(p^n)\big](s \to 0) \sim Cs^{-n-1/2} \ , \tag{7}$$

Violating Froissart bound. General argument gives instead

$$T \sim s^{-\alpha_\Delta(0)} \tag{8}$$

where $\alpha_\Delta(0)$ is the intercept parameter of the Regge trajectory of $\Delta(1232)$. An N/D calculation is nevertheless still doable with

$$\sqrt{s} = (1.01 - 0.19i) \ \mathrm{GeV} \ , \tag{9}$$

within reasonable range of LECs of $\mathcal{O}(p^2)$ lagrangian.

A 'realistic' model calculation

$$\text{disc}\ T(s) = \text{disc}\ T^{(1)}(s) + \text{disc}\ T^{\rho}(s) + \text{disc}\left[\frac{a+bs}{\sqrt{s}}\right] . \tag{10}$$

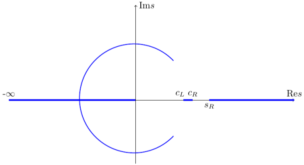

图: The $l.h.c.$ by t-channel ρ exchange; u-channel N exchange.

$$\sqrt{s} = (0.90 - 0.20i)\text{GeV} . \tag{11}$$

$SU(3)$ K matrix approach

[Chen C et al., 2022 CPC]

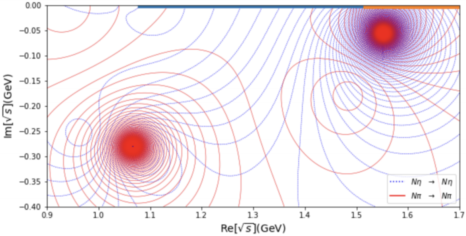

Figure 5: The $N^*(890)$ and $N^*(1535)$ poles in sheet (-,+). The corresponding thresholds are marked with thick lines in the upper edge of the box.

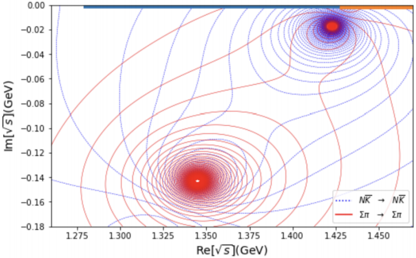

$SU(3)$ K matrix approach

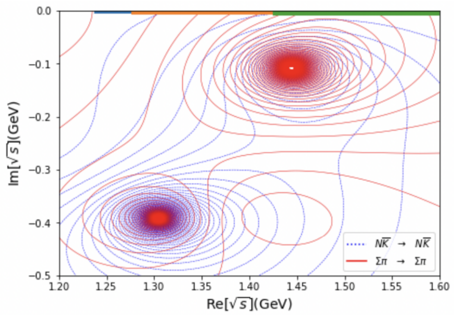

Figure 7: $\Sigma^*(1360)$ and $\Sigma^*(1620)$ poles in sheet (-,-,+).

An $SU(3)$ version of effective lagrangian is written from which a K matrix is extracted. It is found that the negative parity baryon cannot be generated by inputting an 'elementary' filed in the effective lagrangian.

$\gamma(\gamma^*)N \to \pi N$ process

[Ma Y et al., 2021 CPC]

Table 3: Results of $g_\gamma g_\pi$ and g_π^2. Pole position, moduli and phase are in GeV, $10^{-2} \times \mathrm{GeV}^2$ and degrees, in order. g_π^2 are the same for p target and n target due to the isospin symmetry.

		$g_\gamma g_\pi$				g_π^2	
		Fit I		Fit II			
Target	Pole Position	Moduli	Phase	Moduli	Phase	Moduli	Phase
p	$0.882 - 0.190i$	(1.212 ± 0.014)	-79.2 ± 1.3	1.203 ± 0.302	-78.9 ± 11.4	19.7 ± 0.3	32.6 ± 1.0
	$0.960 - 0.192i$	(1.467 ± 0.016)	-71.3 ± 0.9	1.459 ± 0.279	-71.2 ± 3.5	21.4 ± 0.2	33.6 ± 0.8
n	$0.882 - 0.190i$	(0.6416 ± 0.0265)	111 ± 7	2.025 ± 0.731	81.4 ± 6.9		
	$0.960 - 0.192i$	(1.111 ± 0.050)	103 ± 3	2.342 ± 0.605	98.0 ± 1.5		

than that of the $N^*(1535)$ residue. The $|g_\pi^2|$ of $N^*(890)$ is $0.2\mathrm{GeV}^2$, and the one of $N^*(1535)$, which is obtained by the value in Ref. [45], is $0.08\mathrm{GeV}^2$. The g_π^2 of these two resonances may account for part of the reason why $N^*(890)$ photoproduction residue is large, and using above results g_γ of these two resonances can be obtained. The $|g_\gamma|$ of $N^*(890)$ is 0.032GeV meanwhile the one of $N^*(1535)$ is 0.024GeV and one can see the magnitudes are almost the same. One should notice that the results of n target are quiet unstable. The fact that data points are few and they have large error bars may account for the main reason.

Dyson's theorem

设入射和出射核子动量分别为 p, p', 入射和出射 π 介子动量分别为 k, k'. S 矩阵元的 R 乘积:

$$T = -\int d^4 x e^{i\frac{k+k'}{2}x}\langle p'|R\{\phi(\frac{x}{2})\phi(-\frac{x}{2})\}|p\rangle \ , \tag{12}$$

或者

$$T = -\int d^4 x e^{i\frac{k'-p'}{2}x}\langle 0|R\{\phi(\frac{x}{2})\psi(-\frac{x}{2})\}|pk\rangle \ , \tag{13}$$

其中 ϕ 代表介子场, ψ 代表核子场。上面两个公式中, 前一个表达式可以用来推导色散关系, 而后一个则可以用来研究散射振幅对 t 的依赖关系。以上的这些表达式都是推迟格林函数的 Fourier 变换, 或者是对其乘积的求和。我们下面构造出相对应的非推迟对易子的 Fourier 变换:

$$F(q^2) = \int d^4 x e^{iqx}\langle 0|[j(\frac{x}{2}), f(-\frac{x}{2})]|n, p+k\rangle \ , \tag{14}$$

其中 $j = (\Box + M^2)\phi(x)$, $j = (\Box + m^2)\psi(x)$. 如此构造出来的 $F(q^2)$ 是一个在 x 类空区间为零的函数的 Fourier 变换。它在除了以下的动量范围内为零:

$$\frac{p_0+k_0}{2} + q_0 > 0\ ,\ \text{且}\ (\frac{p+k}{2}+q)^2 > m_1^2\ ,$$

或者

$$\frac{p_0+k_0}{2} - q_0 > 0\ ,\ \text{且}\ (\frac{p+k}{2}-q)^2 > m_2^2\ ; \tag{15}$$

其中 m_1, m_2 分别是与 j, f 耦合的最低的中间态质量。

Dyson's theorem

Dyson 的工作[F. J. Dyson, PR (1958)] 找到了这样的函数满足的充分必要的表示:

$$F(q^2) = \int d^4l \int_0^\infty d\chi^2 \varepsilon(q_0 - l_0)\delta[(q-l)^2 - \chi^2]\phi(l, \chi^2)\ . \tag{16}$$

在其中 $\phi(l,\chi^2)$ 取值是任意的，如果 $\frac{p+k}{2}+l$, $\frac{p+k}{2}-l$ 都取在朝前光锥上，并且

$$\chi \geq \mathrm{Max}\{0; m_1 - \sqrt{((p+k)/2+l)^2}; m_2 - \sqrt{((p+k)/2-l)^2}\}\ . \tag{17}$$

推迟格林函数，$F_R(q^2)$，与 $F(q^2)$ 有如下的关系:

$$F_R(q^2) = -\frac{1}{2\pi}\int dq_0' \frac{F(q')}{q_0' - q_0}\ . \tag{18}$$

将 (16) 式代入得

$$F_R(q^2) = -\frac{1}{2\pi}\int d^4l \int \frac{d\chi^2\phi(l,\chi^2)}{(q-l)^2-\chi^2}\ . \tag{19}$$

再将其代入 (12) 式，得到

$$T = \frac{1}{2\pi}\int \frac{d^4l d\chi^2 \phi(l,\chi^2,p,k)}{((k'-p')/2-l)^2-\chi^2}\ . \tag{20}$$

Lehmann ellipse

引入记号

$$W^2 = (p+k)^2 = s\ , \quad q_{s12}^2 = \frac{(s-(m+M)^2)(s-(m-M)^2)}{4s}\ , \tag{21}$$

在 (20) 式中利用极坐标来表示 $\vec{l}$, 可将其改写成

$$T(W, \cos\theta) = \int_{x_0(W)}^{\infty} dx \int_0^{2\pi} d\alpha \frac{\bar{\phi}(x, \cos\alpha, W)}{x - \cos(\theta-\alpha)}\ , \tag{22}$$

其中

$$\begin{aligned} \bar{\phi}(x, \cos\alpha, W) \quad = \quad & -\frac{1}{4\pi q_{s12}} \int dl_0 \int l dl \int d\chi^2 \int d\beta \\ & \times \delta[x - \frac{q_{s12}^2 + l^2 + \chi^2 - (l_0 + (m^2 - M^2)/2W)^2}{2 q_{s12} l \sin\beta}] \\ & \times \phi(l_0, l^2, \cos\alpha\sin\beta, \chi^2, W)\ . \end{aligned} \tag{23}$$

Lehmann Ellipse

通过直接计算可以得出

$$x_0(W) = \left[1 + \frac{(m_1^2 - M^2)(m_2^2 - m^2)}{q_{s12}^2(s - (m_1 - m_2)^2)}\right]^{1/2} , \tag{24}$$

其中 m_1 是与 π 耦合的最低的态的质量，以使得比如 $\langle 1|j(0)|0\rangle \neq 0$. 而对于 m_2 的定义是类似的. 比如有 $m_1 = 3M$, $m_2 = m + M$。在 (22) 式中，由于 $\cos\theta$ 仅仅出现在分母上，我们可以考虑把它作为一个复变量，并且讨论散射矩阵元作为这个变量的解析函数。这种函数的奇异性仅仅当分母为零时才出现，即

$$\cos\theta = x\cos\alpha \pm i\sqrt{x^2-1}\sin\alpha \ . \tag{25}$$

于是我们得到结论：对于固定的物理的入射能量 W, 散射振幅 $T(s,t)$ 是一个关于 $\cos\theta$ 的解析函数, 其解析区域是一个 $\cos\theta$ 平面上的椭圆, 其焦点 (foci) 为 ± 1, 半长轴 (semi-major axis) 为 $x_0(W)$.

Lehmann ellipse

而对于散射振幅的虚部，则其在一个更大的椭圆上解析. 此椭圆焦点 (foci) 为 ± 1, 半长轴 (semi-major axis) 为

$$\bar{x}_0 = 2x_0^2 - 1 \ . \tag{26}$$

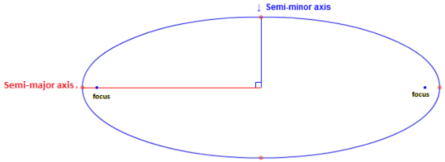

图: Lehmann 椭圆. 半长轴是 x_0, 而焦点是 $\cos\theta = \pm 1$.

注意 x_0 和 $\bar{x}_0$ 均是 s 的函数. 在阈处, $q_{s12}^2 \to 0$, Lehmann 椭圆是整个 $\cos\theta$ 平面. 而当 $s \to \infty$ 时, Lehmann 椭圆会收缩到 (-1,+1).

Lehmann Ellipse

对于 Legendre 级数来说，收敛区间为椭圆是一个自然的结果. 假设级数 $f(z)=\sum_{n=0}^{\infty} a_n z^n$ 的收敛半径为 $|z|<R$, 则 Legendre 级数 $f(z)=\sum_{n=0}^{\infty} a_n P_n(z)$ 收敛于椭圆 $E((R^2+1)2R)$ 内, 半长轴为 $(R^2+1)/2R$. 根据 Legendre 函数的 Laplace 积分公式,

$$P_n(z)=\frac{1}{\pi}\int_0^{\pi}(z+\sqrt{z^2-1}\cos\phi)^n d\phi\ , \tag{27}$$

于是

$$\sum_{n=0}^{\infty} a_n P_n(z)=\frac{1}{\pi}\int_0^{\pi}\sum_0^{\infty} a_n(z+\sqrt{z^2-1}\cos\phi)^n d\phi\ . \tag{28}$$

即 Lengendre 级数的收敛区间由 $|z+\sqrt{z^2-1}\cos\phi|<R$ (对于任意的 ϕ) 决定. 令 $z+\sqrt{z^2-1}=Re^{i\theta}$, $z\equiv x+iy$ 则

$$x=\frac{R^2+1}{2R}\cos\theta\ ,\quad y=\frac{R^2-1}{2R}\sin\theta\ , \tag{29}$$

或者

$$\left(\frac{x}{(R^2+1)/2R}\right)^2+\left(\frac{y}{(R^2-1)/2R}\right)^2=1\ . \tag{30}$$

这是一个半长轴为 $(R^2+1)/2R$ 的椭圆, 而级数 $\sum_0^{\infty} a_n P_n(z)$ 在椭圆里面收敛. 对于 t 平面椭圆的焦点位于 $t=-4q_{s12}^2$, $t=0$. 这个收敛区域在 $q_{s12}\to 0$ 时并不够用: 当 $s\to s_{th}$, $q_{s12}^2\to 0$ 时, $t=-2q_{s12}^2(1-\cos\theta)\propto q_{s12}\to 0$. 但幸运的是对于 $T(s,t)$ 的虚部, $A_s(s,\cos\theta)$, Lehmann 告诉我们有一个更大的半长轴为 $2x_0^2-1$ 的椭圆. 此时 $2x_0^2-1\to\frac{c}{q_{s12}^2}\to\frac{const}{q_{s12}^2}$, 于是我们可以延拓 $A_s(s,\cos\theta)$ 到某个固定的负 t.

Mandelstam 谱表示

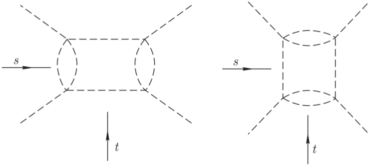

图 7.10　决定 ππ 散射的 Mandelstam 双谱函数 $\rho(s,t)$ 的方块图.

将上两式代入 (7.67) 式并整理得到 (不计入可能的束缚态)

$$
\begin{aligned}
T(s,t,u) = &\frac{1}{\pi^2}\int\int \frac{\rho_{st}(s',t'')}{(s'-s)(t''-t)}\mathrm{d}s'\mathrm{d}t'' + \frac{1}{\pi^2}\int\int \frac{\rho_{su}(s',u'')}{(s'-s)(u''-u)}\mathrm{d}s'\mathrm{d}u'' \\
&+\frac{1}{\pi^2}\int\int \frac{\rho_{tu}(u',t'')}{(u'-u)(t''-t)}\mathrm{d}u'\mathrm{d}t''. \qquad (7.75)
\end{aligned}
$$

Mandelstam 谱表示: $\pi\pi$

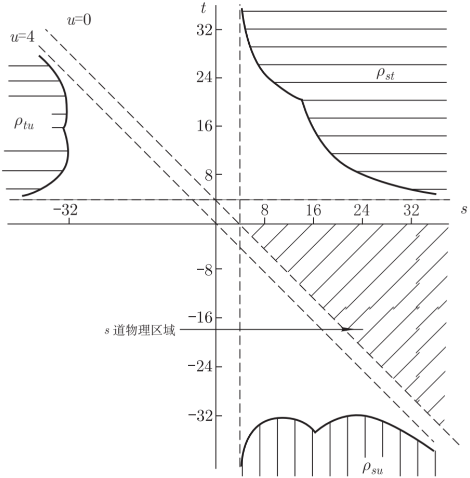

图 7.11 Mandelstam 双谱函数的示意图.

Mandelstam 谱表示： πN

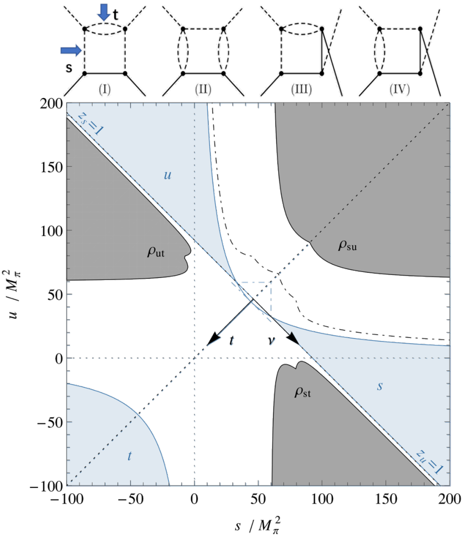

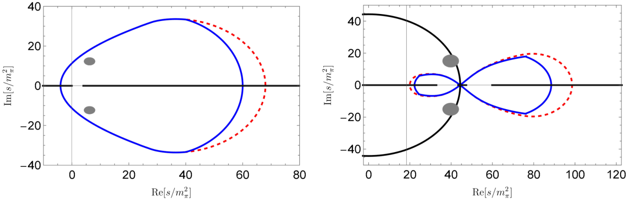

图: 红虚线显示 Mandelstam 解析性给出的 $\pi\pi$，πN 散射固定 t 色散关系的适用范围。蓝线表示 $\pi\pi$，πN 散射由公理化场论给出的适用边界。

Hyperbolic dispersion relations

(a) 曲线需要穿过研究的直接反应道和交叉道的物理区域;

(b) 曲线不能接触到双谱函数非零的区域;

(c) 振幅要尽可能简单，在这个曲线的参数化下最好不要引入运动学割线 (这条起码对于弹性散射要成立);

(d) 分波投影对角度的积分后得到的核应该尽可能简单。

[Hite, Steiner, 1973]

$$(s-a)(u-a)=b$$

a: Influence the domain of validity of equation.

$$\begin{aligned}
A^+(s,t;a) &= \frac{1}{\pi}\int_{s_+}^{\infty} \mathrm{d}s' \left[\frac{1}{s'-s}+\frac{1}{s'-u}-\frac{1}{s'-a}\right] \operatorname{Im} A^+(s',t') + \frac{1}{\pi}\int_{t_\pi}^{\infty} \mathrm{d}t' \frac{\operatorname{Im} A^+(s',t')}{t'-t} \,, \\
A^-(s,t;a) &= \frac{1}{\pi}\int_{s_+}^{\infty} \mathrm{d}s' \left[\frac{1}{s'-s}-\frac{1}{s'-u}\right] \operatorname{Im} A^-(s',t') + \frac{1}{\pi}\int_{t_\pi}^{\infty} \mathrm{d}t' \frac{\nu}{\nu'} \frac{\operatorname{Im} A^-(s',t')}{t'-t} \,, \\
B^+(s,t;a) &= N^+(s,t) + \frac{1}{\pi}\int_{s_+}^{\infty} \mathrm{d}s' \left[\frac{1}{s'-s}-\frac{1}{s'-u}\right] \operatorname{Im} B^+(s',t') + \frac{1}{\pi}\int_{t_\pi}^{\infty} \mathrm{d}t' \frac{\nu}{\nu'} \frac{\operatorname{Im} B^+(s',t')}{t'-t} \,, \\
B^-(s,t;a) &= N^-(s,t;a) + \frac{1}{\pi}\int_{s_+}^{\infty} \mathrm{d}s' \left[\frac{1}{s'-s}+\frac{1}{s'-u}-\frac{1}{s'-a}\right] \operatorname{Im} B^-(s',t') + \frac{1}{\pi}\int_{t_\pi}^{\infty} \mathrm{d}t' \frac{\operatorname{Im} B^-(s',t')}{t'-t} \,.
\end{aligned}$$

Roy equation

Roy Equation [Roy 1971]

- A coupled system of PWDRs.
- Analyticity, Unitarity, and Crossing symmetry.

Starting from the twice-subtracted fixed-t dispersion relation:

$$T(s,t,u)=\alpha(t)+s\beta(t)+\frac{s^2}{\pi}\int_{4m_\pi^2}^{\infty}\mathrm{d}s'\,\frac{\mathrm{Im}\,T(s',t,u')}{s'^2\,(s'-s)}+\frac{s^2}{\pi}\int_{-\infty}^{-t}\mathrm{d}s'\,\frac{\mathrm{Im}\,T(s',t,u')}{s'^2\,(s'-s)}\ , \tag{31}$$

A system of integral equations for the $\pi\pi$ amplitudes:

$$\boxed{\mathrm{Re}\,t_J^I(s)=k_J^I(s)+\sum_{I'}\sum_{J'}\int_{4m_\pi^2}^{\infty}ds'\,K_{JJ'}^{II'}\left(s',s\right)\mathrm{Im}\,t_{J'}^{I'}(s')}\ . \tag{32}$$

- $K_{JJ'}^{II'}\left(s',s\right)$: Analytically calculable kinematic kernel functions.
- The only free parameters: S -wave scattering lengths a_0^0, a_0^2.

An important issue is the range of validity of the Roy equations.

Lehmann ellipse constraints

$$\mathrm{Im}_s\, T\left(s', t\right) = 16\pi \sum_l (2l+1)\, \mathrm{Im}_s\, T_l\left(s'\right) P_l\left(z\left(s', t\right)\right) \ , \tag{33}$$

z : **CMS scattering angle cosines.**

The series of Legendre polynomials converges when z within the corresponding large Lehmann ellipses[Lehmann 1958].

Lehmann ellipses

- Focal points: $z = \pm 1$.
- Boundary: Touching the nearest singularity of $\mathrm{Im}_s\, T\left(s', t\right)$.

Assuming that the scattering amplitude satisfies Mandelstam's double spectral representation.

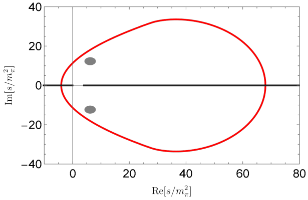

图: Domain of validity of the Roy Equation; black points denote the $\sigma(f_0(500))$.

Similarly, for πK and πN scattering amplitudes:

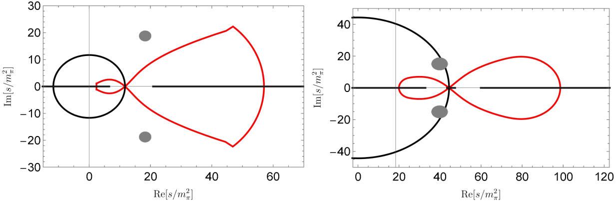

图: Left:πK systems, points denote the $\kappa(K_0^*(700))$; Right: :πN systems, points denote the $N^*(890)$

Roy equation(fixed-t dispersion relation): unfit to search for a wide resonance.

Using the hyperbolic dispersion relations, One can get the Roy-Steiner equations, which looks like:

$$\begin{aligned} \mathrm{Re}\, f_l(s) &= N_l(s) + \sum_{l'} \int_{s_{th}} ds'\, K_{l,l'}(s,s')\, \mathrm{Im}\, f_l(s') + \sum_{J} \int_{t_{th}} dt'\, G_{l,J}(s,t')\, \mathrm{Im}\, g(t')_J\ , \\ \mathrm{Re}\, g_J(t) &= \tilde{N}_J(t) + \sum_{l'} \int_{s_{th}} ds'\, \tilde{K}_{J,l'}(t,s')\, \mathrm{Im}\, f_l(s') + \sum_{J'} \int_{t_{th}} dt'\, \tilde{G}_{J,J'}(t,t')\, \mathrm{Im}\, g(t')_J\ . \end{aligned} \tag{34}$$

- $f_l(s)$: s-channel PWAs;
- $g_J(t)$: t-channel PWAs;
- N, K, G: Analytically calculable kinematic kernel functions.

RS equation analysis of πN scatterings

RS equation has been applied to study πN scatterings[Ditsche:2012,Hoferichter:2015].

- Choosing $a = -23.7m_\pi^2$: The largest domain of validity in real axis. $W \in [1.08GeV, 1.38GeV]$.
- Unable to continue to the complex plane.

Condition of continuation: $a \in (-2.59m_\pi^2, 4m_\pi^2)$

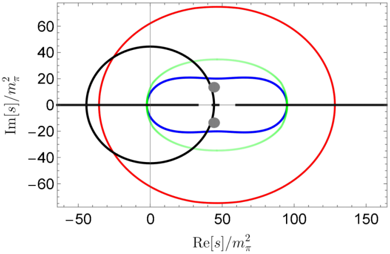

FIG. 2: Validity domain of the fixed-b RS representation ($a = 0$). The blue and green lines correspond to the boundaries in the s' and t' integrals associated with ρ_{st}, respectively. The red line corresponds to the boundaries in the s' integral associated with ρ_{su}.

[Cao XH, Li QZ, HQZ, arXive:2207.09743].

- S_{11}: $\sqrt{s} = 919 \pm 4 - (162 \pm 7)i \quad N^*(920)$.
- P_{33}: $\sqrt{s} = 1213 \pm 2 - (50 \pm 3)i \quad \Delta(1232)$.

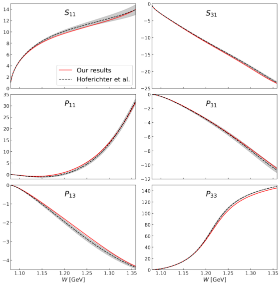

FIG. 3: Phase shifts of the s-channel PWs from our solutions (solid line) and [10] (dashed line with error bands) in the low-energy region. The deviation of P_{33} phase shift comes from the difference between values of GWU/SAID and [10] at the matching point ($W_{\mathrm{m}} = 1.36$ GeV), and they differ by about 2°.

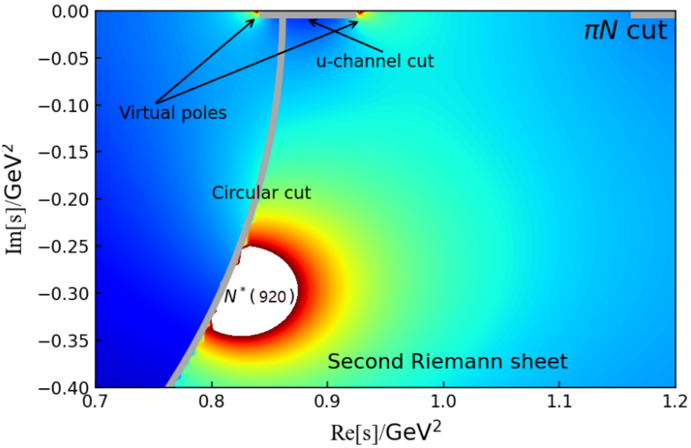

πN cut
u-channel cut
Virtual poles
Circular cut
N*(920)
Second Riemann sheet
Im[s]/GeV²
Re[s]/GeV²
0.00
−0.05
−0.10
−0.15
−0.20
−0.25
−0.30
−0.35
−0.40
0.7
0.8
0.9
1.0
1.1
1.2

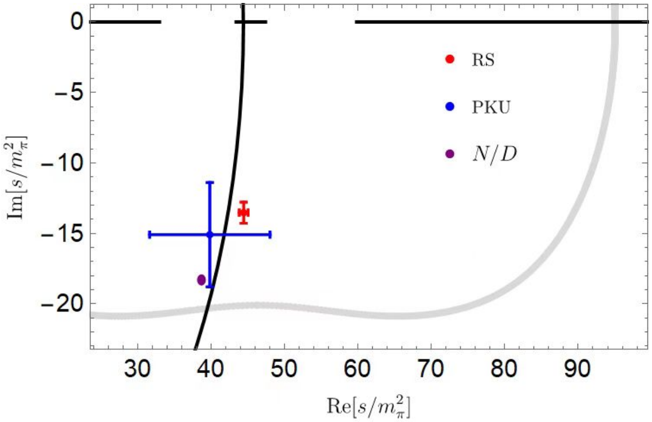

0
−5
−10
−15
−20
30
40
50
60
70
80
90
RS
PKU
N/D
$\mathrm{Im}[s/m_\pi^2]$
$\mathrm{Re}[s/m_\pi^2]$

Virtual poles

The πN scattering amplitudes can be decomposed as:

$$T(\pi^a + N_i \to \pi' + N_f) = \chi_f^\dagger(\delta^{aa'} T^+ + \frac{1}{2}[\tau^{a'}, \tau^a] T^-)\chi_i \ , \tag{35}$$

As for the Lorentz structure,for an isospin index $I \in \{\frac{1}{2}, \frac{3}{2}\}$,

$$T^I = \bar{u}^{(s')}(p')[A^I(s,t) + \frac{1}{2}(\not{q} + \not{q}')]B^I(s,t)]u^{(s)}(p) \ , \tag{36}$$

The u channel nucleon pole term is contained in function $B^I(s,u)$:

$$-\frac{m_N^2 g^2}{F^2}\frac{1}{u - m_N^2} \in B^{1/2}(s,u) \ , \quad \frac{2m_N^2 g^2}{F^2}\frac{1}{u - m_N^2} \in B^{3/2}(s,u) \ . \tag{37}$$

- m_N, g and F denote the nucleon mass,axial vector coupling constant,and pion decay constant.
- the sign and even the value of these parameters are immune of chiral corrections.

After partial wave projection,the pole term leads partial wave amplitudes to behave in the neighbourhood of $c_R = m_N^2 + 2m_\pi^2$ like :

$$\begin{aligned} s \to c_R, \quad & T_{\pm}^{1/2,J} \to \frac{g^2 m_N^2 (m_N^2 + 2m_\pi^2)}{16\pi F^2 (4m_N^2 - m_\pi^2)} \ln \frac{c_R - c_L}{s - c_R} \to \infty \,, \\ s \to c_R, \quad & T_{\pm}^{3/2,J} \to -\frac{g^2 m_N^2 (m_N^2 + 2m_\pi^2)}{8\pi F^2 (4m_N^2 - m_\pi^2)} \ln \frac{c_R - c_L}{s - c_R} \to -\infty \,. \end{aligned} \tag{38}$$

As to $s \to c_L = (m_N^2 - m_\pi^2)^2 / m_N^2$:

- $T_{\pm}^{1/2,J} \to \mp(-1)^{J+1/2}\infty.$
- $T_{\pm}^{3/2,J} \to \pm(-1)^{J+1/2}\infty.$

The parity eigenstates can be obtained by the linear combinations：

$$T_{\pm}^{I,J} = T_{++}^{I,J} \pm T_{+-}^{I,J} \,. \tag{39}$$

Amplitudes $T_{\pm}^{I,J}$ are corresponding to orbital angular momentum $L = J \mp 1/2$ with $P = (-1)^{J \pm 1/2}$.

$$S_{\pm}^{I,J} = 1 + 2i\rho(s)\, T_{\pm}^{I,J} \tag{40}$$

$$\rho(s) = \frac{\sqrt{(s - s_L)(s - s_R)}}{2} \,, s_R = (m_N + m_\pi)^2, s_L = (m_N - m_\pi)^2$$

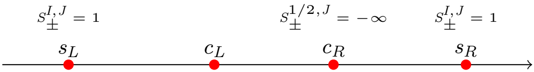

Following the same reasons mentioned above ,we can conclude that:

- $s \in (c_R, s_R)$, the $S_{\pm}^{1/2,J}$ must contain a zero point.
- $s \in (s_L, c_L)$, $S_{+}^{1/2,J}$ and $S_{-}^{3/2,J}$ contain a zero point for J = 1/2, 5/2, 9/2, . . . , while $S_{-}^{1/2,J}$ and $S_{+}^{3/2,J}$ contain a zero point for J = 3/2, 7/2, 11/2, ...

$$T(s,t) = 16\pi \sum_{J=1/2}^{\infty} (2J+1)\, T^J(s)\, d^J_{1/2,-1/2}(\cos\theta) \ ,$$

$$T^{\mathrm{II}}_{+\pm}(s,t) = 8\pi \sum_{J=1/2} (2J+1) \left[\frac{T^J_+(s)}{S^J_+(s)} \pm \frac{T^J_-(s)}{S^J_-(s)} \right] d^J_{1/2,\pm 1/2}(\cos\theta)$$

$s = c_L, c_R$, are accumulation of poles on sheet II, and form two nonisolated singularities of $T(s,t)$ on sheet II.

[Li QZ, HQZ, arXive: 2108.03734] CTP to appear

Seen by numerical solutions of RS equation!

Also the virtual pole accompanying nucleon!

Regge Trajectory